Available online at www.sciencedirect.com
SCIENCE DIRECT
Polymer 47 (2006) 6218–6225
polymer
www.elsevier.com/locate/polymer

Analysis of micro-failure behaviors in hybrid fiber model composites

Shifang Luan [a,1], Hongzhou Li [a,1], Yuxi Jia [a], Lijia An [a], Yanchun Han [a,*], Qian Xiang [b], Jiang Zhao [b], Junxing Li [b], Charles C. Han [b,*]

[a] State Key Laboratory of Polymer Physics and Chemistry, Changchun Institute of Applied Chemistry, Graduate School of Chinese Academy of Sciences, Changchun 130022, PR China
[b] State Key Laboratory of Polymer Physics and Chemistry, Institute of Chemistry, Chinese Academy of Sciences, Beijing 100080, PR China

Received 24 April 2006; received in revised form 14 June 2006; accepted 14 June 2006
Available online 14 July 2006

Abstract

Micro-failure modes and statistical fragment lengths in the hybrid fiber and non-hybrid reference composites in the uniaxial tension were investigated. Similar to the reference experiments, fibers in hybrid strong interface/medium interface fiber composites display a decrease in aspect ratio and an increase in interfacial shear stress (IFSS) with the increase of inter-fiber spacing. While for the fibers with weak interfaces in the hybrid strong interface/weak interface fiber composites, the aspect ratio increases and IFSS decreases with enlargement of inter-fiber spacing, which is contrary to other systems. Finite element numerical analysis was used to interpret the special phenomena.

Keywords: Fiber–fiber interaction; Hybrid fiber composites; Finite element analysis

1. Introduction

Hybrid fiber composite, which consists of more than one type of fibers, exhibits a complex combination of micro-failure modes, such as fiber breakage, interfacial debonding, and delamination. Thus, optimization of its stiffness, strength, and elongation can be reached [1–16]. Bader et al. found that up to 40% strength increase and 50% failure strain enhancement could be obtained in hybrid glass fiber/carbon fiber composites [3–6]. Fiber–matrix stress transfer and fiber–fiber interaction in hybrid fiber composites have been generally accepted as the predominant parameters in controlling micro-failure modes, also recognized as the most important influencing factors in macroscopic mechanical behavior of fiber-reinforced materials. However, there has been rare report on such related studies due to the difficulties in preparation and characterization of well-defined model specimens [17,18]. It is only recently that the two-dimensional multi-fiber model composites began to be widely applied to examine the micromechanics of fiber composites. Techniques such as polarized light microscopy [18–21], Raman and fluorescence spectroscopy [15,16,22–29] are used to examine the effects of inter-fiber spacing, fiber–matrix interfacial strength and matrix plasticity on the stress concentration factor (SCF) and fiber failure process. From model composites, intrinsic information about stress concentration, fiber–fiber and fiber–matrix interactions, as well as initiation of micro-failure can be acquired [13–17]. Jones and DiBenedetto found that among AS-4 carbon/IM6-G carbon, A-1110 E-glass/A-163 E-glass, Kevlar-49/AS-4 carbon, and A-1110 E-glass/AS-4 carbon systems, the least amount of coordinated fracture appeared in carbon fiber/Kevlar fiber hybrid system, and these results were in good agreement with those computer simulation results based on the local load sharing principles [17]. Grubb et al. discovered that the load transfer length measured by Raman spectroscopy agreed well with that given by the photoelastic method in the hybrid carbon fiber/Kevlar fiber composites. However, the stress concentration factors were

* Corresponding authors. Tel.: +86 10 82618089; fax: +86 10 62521519.
E-mail addresses: ychan@ciac.jl.cn (Y. Han), c.c.han@iccas.ac.cn (C.C. Han).
[1] Ph.D. student of Graduate School of Chinese Academy of Sciences. They contributed equally to this work.

0032-3861/$ - see front matter © 2006 Elsevier Ltd. All rights reserved.
doi:10.1016/j.polymer.2006.06.041

in poor agreement with the local load sharing rule and predications made by Eitan and Wagner [16]. It is worth to mention that some important issues, such as the influence of inter-fiber spacing, interfacial strength and matrix properties on the micro-failure phenomena in the hybrid composites, have rarely been considered.

This paper describes a systematic investigation of the micro-failure modes and micromechanical properties in the hybrid E-glass fiber composites. Micro-failure phenomena and statistics of fiber fragmentation in model composites with inter-fiber spacing of 1–8 fiber diameter were investigated. Also, the experimental results were theoretically interpreted by finite element numerical analysis.

2. Experimental

2.1. Materials

E-glass fibers with different sizings were provided by Taian Glass Fiber Co., China. The main components of polymer matrix were diglycidyl ether of bisphenol-A (DGEBA) epoxy (Taiwan Nanya Epoxy Resin Co.) and polypropylenediamine D230 curing agents (BASF).

2.2. Preparation of model specimens

The single fiber and multi-fiber specimens were prepared by a home-made fiber positioning apparatus, as shown in Fig. 1. Unlike fiber positioning methods reported by other groups [7,13,17,21,30,31], the fiber arrays are controlled much more precisely and the operation is more convenient.

The scheduled inter-fiber spacing, S, is calculated according to the following formula:

$$S = \gamma d/R$$

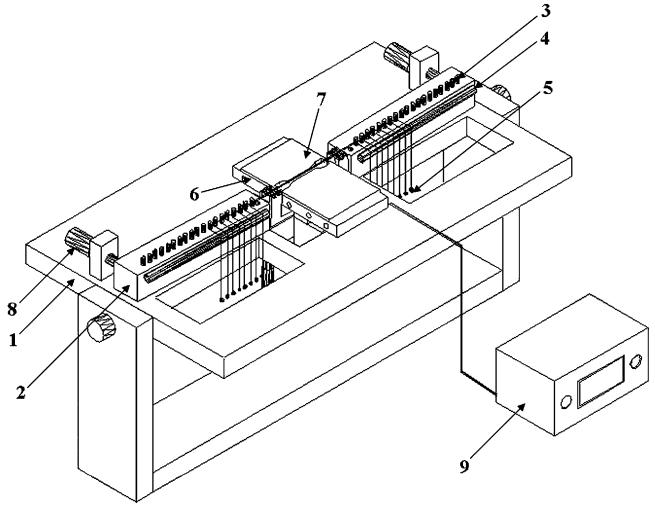

Fig. 1. Schematic of the fiber positioning apparatus. (1) Base panel, (2) rotation rectangular bars, (3) positioning pillar, (4) buffering rod, (5) weight loading, (6) thermo-stage, (7) mold, (8) micrometer stop, and (9) temperature control system.

where R is the rotation radius (distance between the rotation center and the driving point on the micrometer), γ is the center–center distance of the adjacent positioning pillars, and d is the position change value on the micrometer. The estimated positioning error can go down to about 0.1 μm according to the sample requirement. After the alignment of the fiber arrays was finished, a steel mold precoated with fluoride materials was elevated carefully so that all the fibers were embedded at the center of the mold. The degassed mixture of epoxy and its curing agent was poured into the mold, precured for 2 h at 80 °C, and postcured for 3 h at 120 °C.

2.3. Specimens testing

Gauge with a length of 20.0 mm in the central region of the specimens was labeled as the testing target zone, and then specimens were strained using a computer-controlled tensile tester equipped with a high-sensitivity load cell, a high-precision actuator and an optical microscope. Photographs of micro-failures within the monitored gauge-length were taken via the microscope with a polarizer attachment, and then fiber breaks were analyzed.

2.4. Interfacial shear stress measurement

Interfacial shear stress is calculated from the fragmentation test data using the Kelly–Tyson equation [32]:

$$\tau = K\frac{\sigma_{f(l_c)}}{2\bar{l}_c}d_f \quad (1)$$

where τ, $\sigma_{f(l_c)}$, d_f, $\bar{l}_c$ represent the average interfacial shear stress, the fiber tensile strength at the critical fragment length, the fiber diameter, and the mean critical fragment length, respectively. When the fragment length varies between $l_c/2$ and l_c, K adopts a mean value of 3/4. The fiber tensile strength, $\sigma_{f(l_c)}$, at the fiber critical length is calculated from the following equation [33]:

$$\sigma_{f(l_c)} = \sigma_0(l_0/\bar{l}_c)^{1/\rho} \quad (2)$$

where σ_0 denotes the fiber strength at the gauge-length l_0, and ρ the Weibull shape parameter (the Weibull modulus), describing the statistical spread in strength, which is evaluated from the linearized function of the mean fragment length versus fiber stress.

3. Results and discussion

3.1. Micro-failure modes

Physical and mechanical parameters of E-glass fibers and epoxy matrix are presented in Table 1.

3.1.1. Micro-failure modes of non-hybrid fibers

Three kinds of E-glass fibers coated with silane, mixture of silane and urethane, and urethane sizings, were used to prepare specimens with different interfacial strengths, i.e. strong

Table 1
Physical and mechanical parameters of the E-glass fibers and the epoxy matrix

Parameters	E-glass 1	E-glass 2	E-glass 3	Epoxy
Diameter (μm)	24 ± 1.1	17 ± 0.7	19 ± 0.8	–
Tensile strength (MPa)	2030 ± 60	2220 ± 80	2300 ± 70	61.0 ± 0.7
Tensile modulus (GPa)	72.5 ± 3.8	74.1 ± 5.4	74.3 ± 4.7	1.9 ± 0.1
Elongation (%)	2.4 ± 0.3	2.6 ± 0.2	2.6 ± 0.2	8.4 ± 0.6
Poisson ratio, ν	~0.22	~0.22	~0.22	~0.4
Surface treatment	Silane	Mixture[a]	Urethane	–

[a] Mixture was composed of silane and urethane sizings.

interface, medium interface, and weak interface, respectively. When fibers are separated far away from each other, the fiber–fiber interaction becomes so weak that their fracture is mainly dominated by the defects within the fibers themselves and a random fracture is exhibited. When fiber–fiber interaction is strong enough, coordination fracture is the dominating feature, indicating that the stress concentrations caused by primary fiber fractures are sufficiently high to bring about fracture of the adjacent fiber in the proximity of the fiber breaks. Quantitatively, the coordination fracture is defined as the situation that the frequency of the maximum aligned breaks within 15% of the critical length of the fiber is over 35% for each specimen, identical to the definition reported by other groups [18].

As shown by the micro-failure patterns in the strong interface specimens (Fig. 2a–d), the strong birefringence nodes initiated from the breaks, and propagated along the fiber axis (Fig. 2d). In the direction perpendicular to the fiber axis at the distance within one times of the fiber diameter (denoted as 1*D*), the stress concentration was larger than in any other

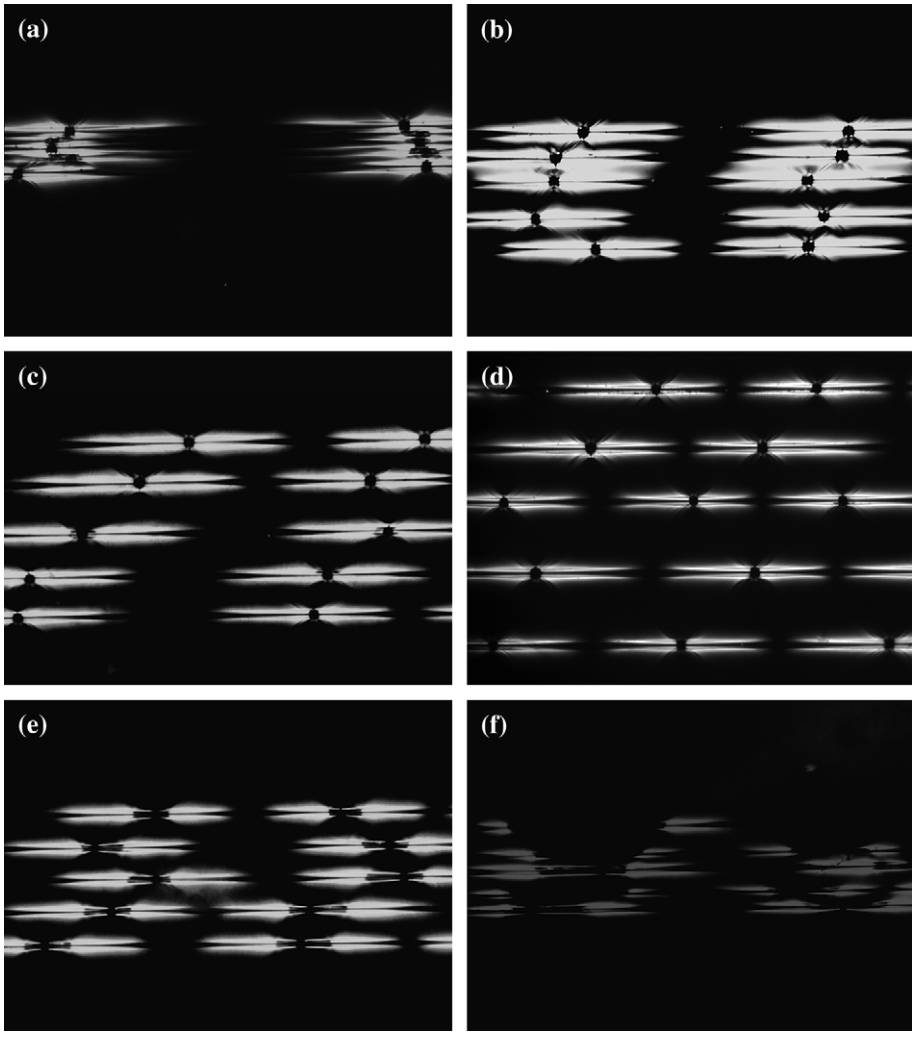

Fig. 2. Polarized photomicrographs showing the fiber failure patterns in the five-fiber specimens. Fibers with strong interface separated by 0.4*D* (a), 3.2*D* (b), 5.0*D* (c), and 7.8*D* (d). Fibers with medium interfaces separated by 4.9*D* (e). Fibers with weak interface separated by 3.5*D* (f).

directions [34]. Thus, these specimens revealed a vertical clustering fracture (Fig. 2a). Coordination fracture line, i.e., the line connecting adjacent fiber breaks, changed from being perpendicular to the fiber axis to parallel as the inter-fiber spacing increased (Fig. 2b and c). When the inter-spacing reached up to $\sim 8D$, the stress concentration around the break became too weak to cause the adjacent fiber fracture. In this case, the fiber fractures displayed a random fracture behavior which was mainly governed by the flaws. According to the quantitative analysis as shown in Fig. 3a, the frequency of five-fiber-coordination fracture faded with inter-fiber spacing increasing.

For medium interface composites, the short birefringence sheaths surrounding the fiber appeared due to the partial debonding (Fig. 2e). Weak interface composites displayed longer birefringence sheaths and shorter birefringence nodes owing to the stronger debonding (Fig. 2f). Medium interface composites presented the random fracture at the inter-fiber spacing up to $\sim 5D$ (Fig. 2e), whereas weak interface composites showed the random fracture behavior when the distance reached just $\sim 3D$ (Fig. 2f). These results revealed that the fiber–fiber interaction faded with the reduction of interfacial strength. Correspondingly, the frequency of five-fiber-coordination fracture decreased with the reduction of interfacial strength (Fig. 3b).

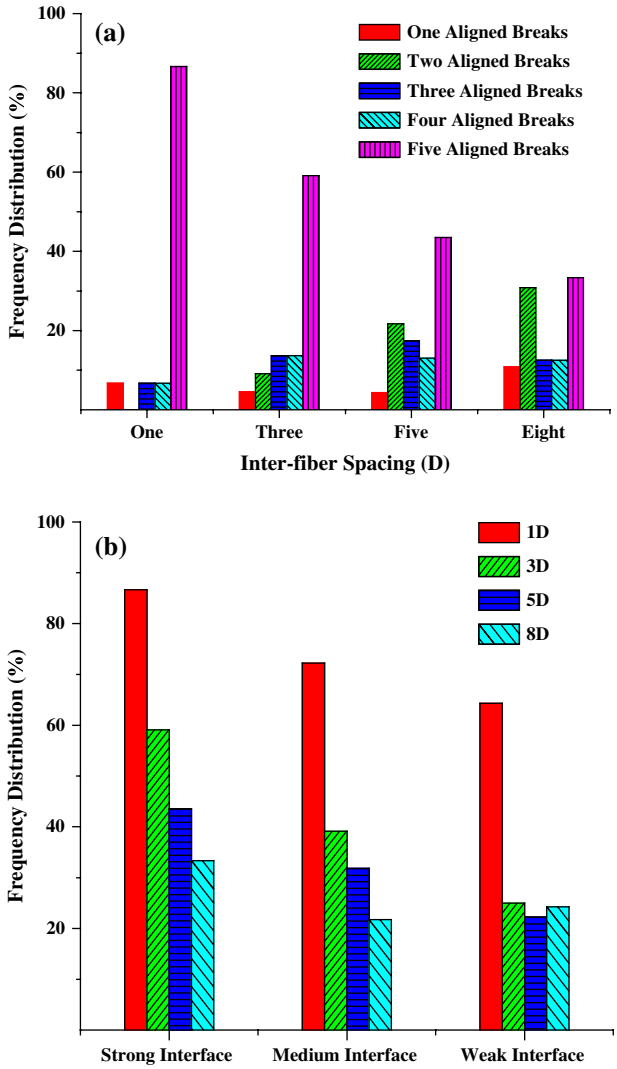

Fig. 3. The coordination fracture of fibers in the non-hybrid five-fiber composites. (a) The influence of inter-fiber spacing on the coordination fracture in strong interface composites; (b) the influence of the interfacial strength on the five-fiber-coordination fracture in the composites.

3.1.2. Micro-failure modes of hybrid fibers

Conventionally, the hybrid fiber composite is referred to a special kind of composites containing more than one type of fibers. The strength and failure characteristics of hybrid fiber composites are controlled by many factors such as fiber type, matrix type, fiber architecture, fiber–matrix interface properties, etc., among which, the interface has been widely recognized as a critical factor [35–37]. In our model hybrid composites, the fibers were made of the same material but had different interfacial strengths. In this way, the interfacial strength effect may be investigated exclusively without considering other factors and the originally complicated systems were expected to be simplified greatly.

Among the five-fiber arrays, the fibers were defined as Fibers 1–5 from the top to the bottom of the hybrid specimens. One type of hybrid composite was composed of three fibers with strong interface, Fibers 1, 3 and 5, and two fibers with medium interface, Fibers 2 and 4 (Fig. 4). The other type of hybrid composite consisted of three fibers with strong interface, Fibers 1, 3, and 5, and two fibers with weak interface, Fibers 2 and 4 (shown in Fig. 5).

As shown in Fig. 4, hybrid strong interface/medium interface fiber composites demonstrated a clustering fracture at the inter-fiber spacing of $\sim 1D$, a coordination fracture at the inter-fiber spacing of $\sim 3D$, and a random fracture at larger inter-fiber spacings. While hybrid strong interface/weak interface system demonstrated a clustering fracture at the inter-fiber spacing of $\sim 1D$, a random fracture at larger inter-fiber spacings was observed due to the existence of fibers with weak interface (Fig. 5). As shown in Fig. 6, the frequencies of coordination fracture in these hybrid fiber systems were larger than 80% at the inter-fiber spacing of $\sim 1D$, and this is similar to that of the non-hybrid strong interface, and greatly larger than that of the non-hybrid medium interface and weak interface composites. This suggests that fiber–fiber interaction is dominated by the fibers with the stronger interface at narrow inter-fiber spacings. As a whole, the frequency of five-fiber-coordination fracture in the hybrid composites decreased with the enlargement of inter-fiber spacing. Compared with the hybrid strong interface/medium interface composites, the hybrid strong interface/weak interface composite exhibited lower frequency of coordination fracture due to fibers with weak interface.

3.2. Statistical fragment length

Here, one-way analysis of variance (ANOVA) is used to make the statistical evaluation on the fragment data [38]. According to ANOVA, at the 95% confidence level, the p-values

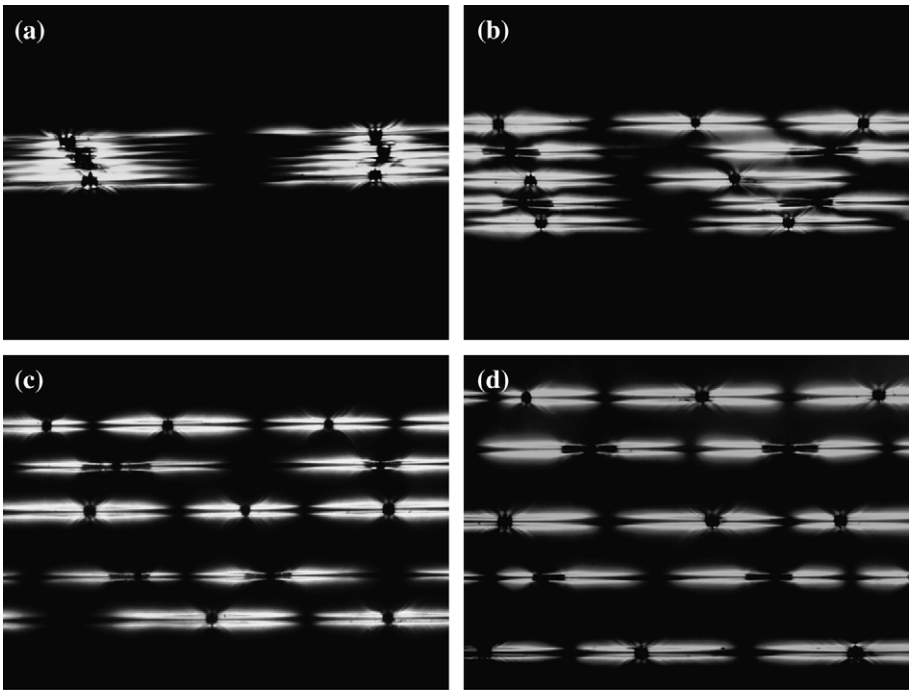

Fig. 4. Polarized photomicrographs of fiber fractures in hybrid strong interface/medium interface composites. Fibers are separated by 0.6*D* (a), 2.9*D* (b), 5.6*D* (c), and 7.9*D* (d).

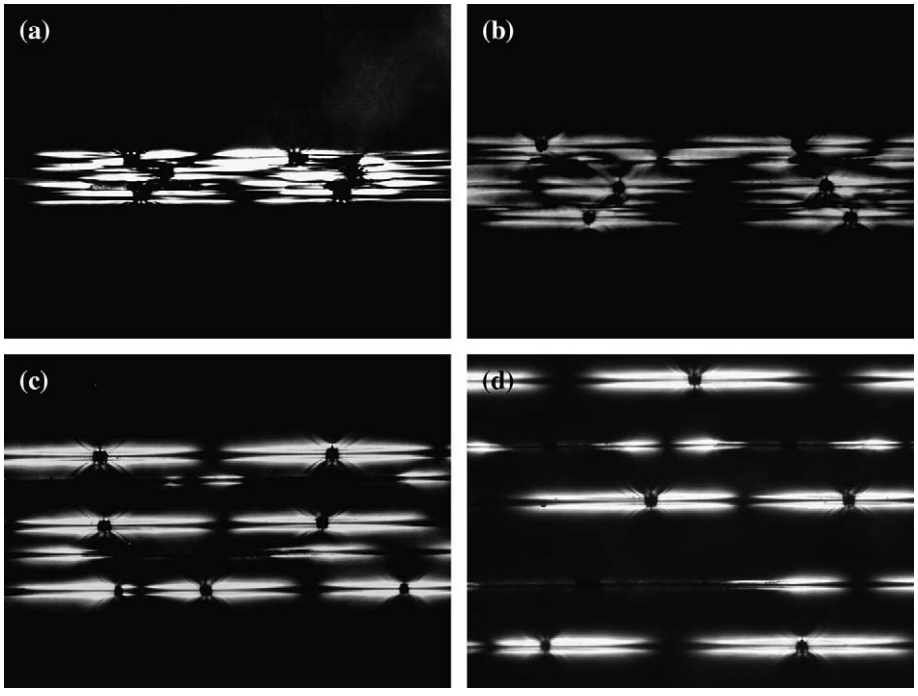

Fig. 5. Polarized photomicrographs showing the fiber failure patterns in hybrid strong interface/weak interface specimens. Fibers are separated by 0.6*D* (a), 2.4*D* (b), 4.5*D* (c), and 8.3*D* (d).

of 0.05 or less are considered statistically as significant difference, and the *p*-values greater than 0.05 are regarded as no significant difference from a statistical viewpoint. The statistical evaluation on the fragment lengths shows that, compared with their corresponding single fiber specimens, the *p*-values increased with inter-fiber spacing in the case of fibers with strong interface and fibers with medium interface in non-hybrid composites. However, for fibers with weak interfaces, such behavior could not be observed (Table 2). Statistical difference may be mainly caused by the strong fiber–fiber interaction. Thus, five-fiber diameters' spacing in the strong interface specimens may be considered as the maximal region,

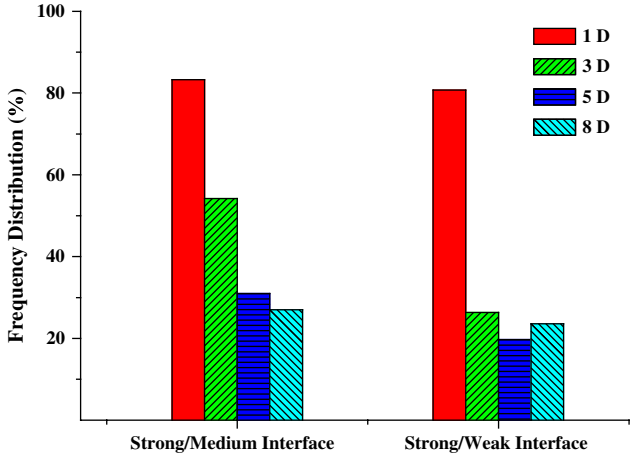

Fig. 6. Five-fiber-coordination fracture in the hybrid fiber composites.

Table 2
p-Values obtained with one-way analysis of the variance for the non-hybrid composites[a]

Inter-fiber spacing (*D*)	1	3	5	8
Strong interface composites	3.3E-10	0.01	0.07	0.41
Medium interface composites	7.6E-4	0.28	0.72	0.81
Weak interface composites	0.78	0.57	0.77	0.60

[a] Related to respective single fiber specimens.

in which a strong interaction between the fibers took place. For the medium interface specimen, the strong interaction region decreased to only about one fiber diameter, while the weak interface specimen showed no strong interaction region at all.

The fibers in the non-hybrid and hybrid strong interface/medium interface fiber systems exhibited the similar effect of inter-fiber spacing on aspect ratio and IFSS. Thus, just four representative curves were illustrated in Fig. 7. The data points at "∞" represent results from the single fiber specimens. It is shown that, except for fibers with weak interface in the hybrid strong interface/weak interface composites, fibers in the non-hybrid and other hybrid systems displayed the similar results, i.e., the aspect ratio decreased and IFSS increased with enlargement of inter-fiber spacing. While fibers with weak interface in the hybrid strong interface/weak interface composites presented the contrary results, i.e., the aspect ratio became larger and IFSS smaller with the increase of the inter-fiber spacing. Besides, in comparison with their respective non-hybrid reference composites, fibers with weak interfaces presented a statistically significant difference at the inter-fiber spacings of 1−5*D* (Table 3). However, in the hybrid strong interface/medium interface composites, both fibers with strong interfaces and fibers with medium interfaces did not show any statistically significant difference, corresponding to their respective non-hybrid reference specimens (Table 3). Obviously, fiber−fiber interactions in this hybrid strong interface/weak interface composites differed from that in the other composites, and the micro-failure behaviors of fibers seem to be affected by the fiber hybrid as well as by the interfacial strength.

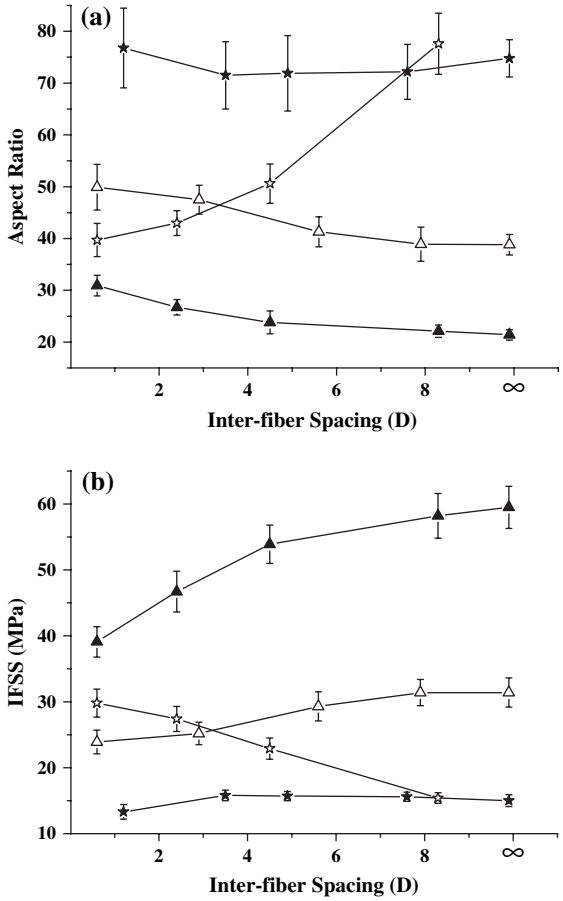

Fig. 7. Effect of inter-fiber spacing on the aspect ratio (a) and IFSS (b) in the specimens. ▲: Fibers with strong interfaces in the hybrid strong interface/weak interface fiber composites; △: fibers with medium interfaces in the hybrid strong interface/medium interface fiber composites; ★: fibers with weak interfaces in the non-hybrid composites; ☆: fibers with weak interfaces in the hybrid strong interface/weak interface fiber composites.

Table 3
p-Values obtained with one-way analysis of the variance for the hybrid composites

Inter-fiber spacing (*D*)	1	3	5	8
Fibers with strong interface[a]	0.26	0.34	0.23	0.86
Fibers with strong interface[b]	0.01	0.73	0.56	0.61
Fibers with medium interface[c]	0.34	0.14	0.32	0.94
Fibers with weak interface[d]	2.3E-5	9.4E-5	1.0E-3	0.44

[a] In the hybrid strong interface/medium interface fiber composites.
[b] In the hybrid strong interface/weak interface fiber composites.
[c] In the hybrid strong interface/medium interface fiber composites.
[d] In the hybrid strong interface/weak interface fiber composites.

3.3. Numerical analysis

In order to interpret theoretically the phenomena described above, the numerical simulation of mesoscopic-mechanical behaviors was conducted, based on the finite element method and Monte Carlo method [39].

From the Mises equivalent stress distribution of broken fibers in non-hybrid strong interface composites (Fig. 8), it

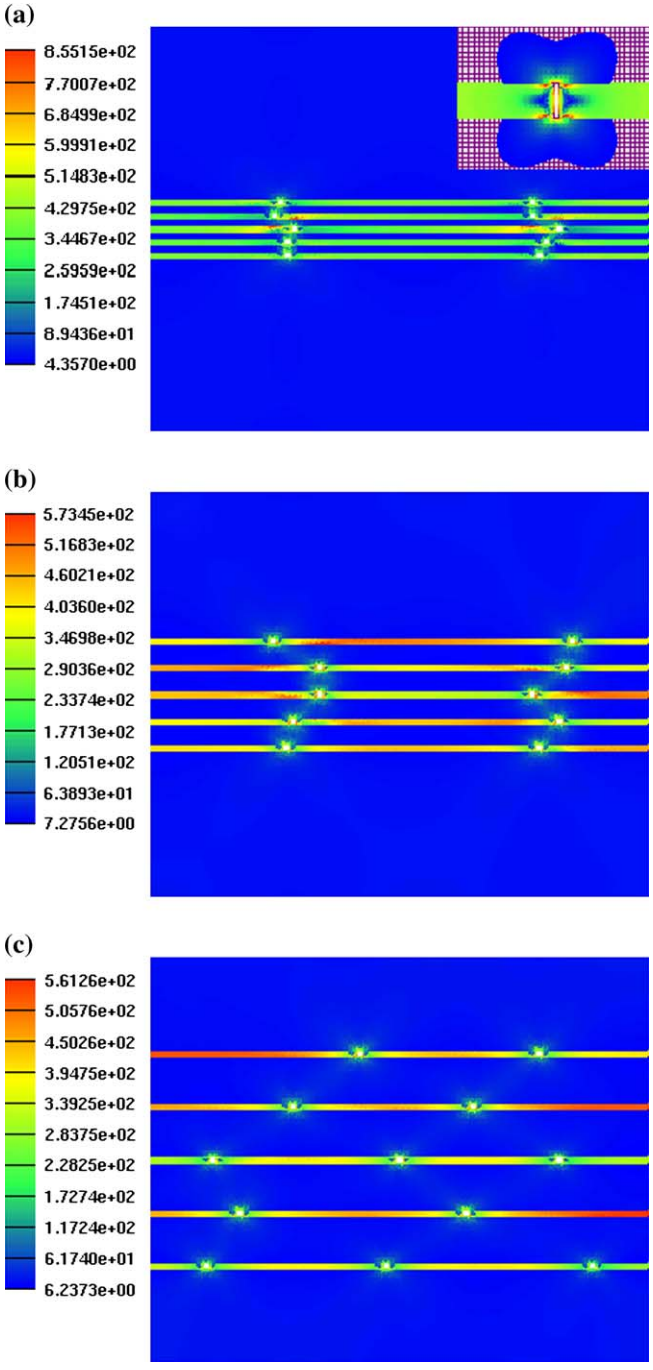

Fig. 8. Mises equivalent stress distribution of fibers with strong interfaces in the non-hybrid composites (unit: MPa). Fibers are separated by 1*D* (a) (the inset photo shows the stress distribution around the breaks of fibers with strong interfaces), 3*D* (b), and 7*D* (c).

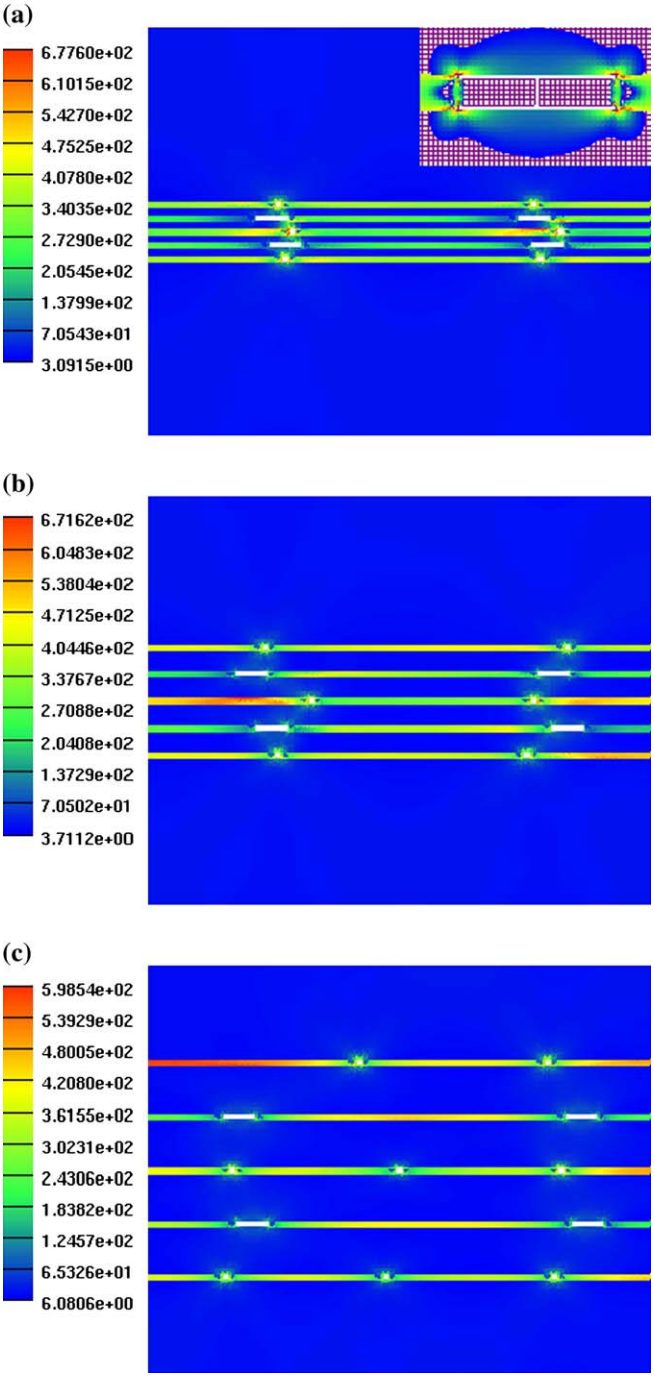

Fig. 9. Mises equivalent stress distribution of broken fibers in hybrid strong interface/weak interface composites. Fibers are separated by 1*D* (a) (the inset photo shows the stress distribution around the breaks of fibers with weak interface), 3*D* (b), and 7*D* (c).

can be seen that the effective loading length of the broken fibers decreased with the enlargement of inter-fiber spacing. Therefore, the aspect ratio of the broken fibers also decreased. According to Eq. (1), with the decrease of the aspect ratio, the IFSS increased. For the hybrid strong interface/medium interface composites, it exhibited the similar failure phenomena due to the small difference of interfacial strength between the fibers with strong interface and the fibers with medium interface.

The Mises equivalent stress distribution of broken fibers in the hybrid strong interface/weak interface composites is shown in Fig. 9. As the inter-fiber spacing increased, the effective loading length of broken fibers with weak interface increased due to the existence of fibers with strong interfaces. Owing to the large difference between the two types of fibers, the tensile load was mainly carried by the fibers with strong interfaces, and then the effective loading length of the broken fibers with weak interfaces became larger. Therefore, the

aspect ratio of the broken fibers with weak interfaces was also increased, and the IFSS of the broken fibers decreased accordingly.

4. Conclusions

Micro-failure modes and statistical fragment lengths in the hybrid fiber were investigated. For hybrid fiber model composites with strong interface/medium interface, their aspect ratio decreases while IFSS increases with the enlargement of inter-fiber spacing, which is similar to non-hybrid specimens. But for fibers with weak interfaces in hybrid strong interface/weak interface fiber composites, their failure behaviors are unusual and contrary to those in the above composites.

Finite element analysis demonstrates that the tensile load along the fiber axis is mainly undertaken by the fibers with strong interface in the hybrid strong interface/weak interface specimens. Therefore, the effective loading length as well as the aspect ratio of fibers with weak interface increases, and the interfacial shear stress decreases with the increase of inter-fiber spacing.

Acknowledgements

This work was supported by the Special Funds of National Basic Research Program by the Ministry of Science and Technology of China (2003CB615600).

References

[1] Bunsell AR, Harris B. Composites 1974;5:157.
[2] Aveston J, Sillwood JM. J Mater Sci 1976;11:1877.
[3] Bader MG, Mander PW. J Mater Sci 1981;16:2233.
[4] Bader MG, Mander PW. J Mater Sci 1981;16:2246.
[5] Pitkethly MJ, Bader MG. J Phys D Appl Phys 1987;20:315.
[6] Bader MG. Sci Eng Compos Mater 1988;1:1.
[7] Gulino R, Schwartz P, Phoenix SL. J Mater Sci 1989;24:6655.
[8] Kobelev VV. Int J Solids Struct 1993;30(3):413.
[9] Roerden AM, Herakovich CT. Compos Sci Technol 2000;60:2443.
[10] Baburaj V, Matsuzaki Y, Nae FA, Ikeda T. J Intell Mater Syst Struct 2001;12(4):259.
[11] Banthia N, Nandakumar N. Cement Concr Compos 2003;25:3.
[12] Tepfers R, Tamuzs V, Apinis R, Vilks U, Modniks J. Mech Compos Mater 1996;32(2):113.
[13] Wagner HD, Steenbakkers LW. J Mater Sci 1989;24:3956.
[14] Wagner HD, Rubbins M, Marom G. Polym Compos 1991;12:233.
[15] Zhou XF, Wanger HD. Compos Sci Technol 2000;60:367.
[16] Grubb DT, Li ZF, Phoenix SL. Compos Sci Technol 1995;54:237.
[17] Jones KD, DiBenedetto AT. Compos Sci Technol 1994;51:53.
[18] Van den Heuvel PWJ, Van der Bruggen YJW, Peijs T. Composites Part A 1996;27A:855.
[19] Holmes GA, Mcdonough WG, Dunkers JP, Han CC. J Polym Sci Part B Polym Phys 2003;41:2976.
[20] Li ZF, Grubb DT, Phoenix SL. Compos Sci Technol 1995;54:251.
[21] Park JM, Kim JW, Goda K. Compos Sci Technol 2000;60:439.
[22] Van den Heuvel PWJ, Peijs T, Young RJ. Compos Sci Technol 1997; 57:899.
[23] Mahiou H, Beakou A, Young RJ. J Mater Sci 1999;34:6069.
[24] Chohan V, Galiotis C. Composites Part A 1996;27A:881.
[25] Schadler LS, Amer MS, Iskandarani B. Mech Mater 1996;23:205.
[26] Wanger HD, Amer MS, Schadler LS. J Mater Sci 1996;31:1165.
[27] Van den Heuvel PWJ, Peijs T, Young RJ. Compos Sci Technol 1998; 58:933.
[28] Chohan V, Galiotis C. Compos Sci Technol 1997;57:1089.
[29] Van den Heuvel PWJ, Peijs T, Young RJ. Composites Part A 2000; 31A:165.
[30] Li ZF, Grubb DT, Phoenix SL. J Mater Sci Lett 1994;13:1720.
[31] Vejen N, Pyrz R. Composites Part B 2001;32B:557.
[32] Kelly A, Tyson WR. J Mech Phys Solids 1965;13:329.
[33] Khalili A, Kromp K. J Mater Sci 1991;26:6741.
[34] Li HZ, Jia YX, Mamtimin G, Wang X, Jiang W, An LJ. Macromol Mater Eng 2006;291:510.
[35] Zinck P, Wagner HD, Salmon L, Gerard JF. Polymer 2001;42:5401.
[36] Zinck P, Wagner HD, Salmon L, Gerard JF. Polymer 2001;42:6641.
[37] Fu SY, Yue CY, Hu X, Mai YW. Compos Sci Technol 2000;60:3001.
[38] Xiong XJ, Arthur JA, Penn LS. Polym Compos 2001;22:349.
[39] Li HZ, Jia YX, Mamtimin G, Jiang W, An LJ. J Appl Polym Sci, in press.